

Instantons and Fluctuations in a Lagrangian Model of Turbulence

G.B. Apolinário¹, L. Moriconi¹, and R.M. Pereira²

¹*Instituto de Física, Universidade Federal do Rio de Janeiro,*

C.P. 68528, CEP: 21945-970, Rio de Janeiro, RJ, Brazil and

²*Laboratório de Física Teórica e Computacional, Departamento de Física,*

Universidade Federal de Pernambuco, 50670-901, Recife, PE, Brazil

Abstract

We perform a detailed analytical study of the Recent Fluid Deformation (RFD) model for the onset of Lagrangian intermittency, within the context of the Martin-Siggia-Rose (MSR) path integral formalism. The model is based, as a key point, upon local closures for the pressure Hessian and the viscous dissipation terms in the stochastic dynamical equations for the velocity gradient tensor. We carry out a power counting hierarchical classification of the several perturbative contributions associated to fluctuations around the instanton-evaluated MSR action, along the lines of the cumulant expansion. The most relevant Feynman diagrams are then integrated out into the renormalized effective action, for the computation of velocity gradient probability distribution functions (vgPDFs). While the subleading perturbative corrections do not affect the global shape of the vgPDFs in an appreciable qualitative way, it turns out that they have a significant role in the accurate description of their non-Gaussian cores.

I. INTRODUCTION

The non-Gaussian statistical behavior of Galilean-invariant turbulent observables, like inertial range velocity differences or velocity gradients – the hallmark of intermittency [1] – is a long standing theoretical problem, ultimately related to the existence of nonlocal interactions between eddies defined at well-separated spacetime scales across the turbulent energy cascade [2].

Fat-tailed velocity gradient probability distribution functions (vgPDFs) are objects of particular interest in the statistical theory of turbulence [3–5]. A main source of motivation has been provided with the introduction, since the mid-1990s, of improved experimental techniques for the measurement of all of the velocity gradient tensor components, based on specific designs of nine and twelve-sensor hot wire probes [6–11]. It is interesting to remark that the vgPDFs obtained from these experiments can have their Reynolds number dependence accurately modeled by the phenomenological log-Poisson cascade picture of intermittency [12], which was originally addressed in the context of velocity structure functions [13, 14].

Taking into account the fact that the Navier-Stokes equations are nonlocal and non-linear in physical space, and that at high Reynold’s numbers they lead to strong coupling regimes, the Lagrangian picture of the flow comes into play as a promising stage for a deeper understanding of intermittency. From a purely mathematical perspective, the Lagrangian viewpoint is a natural approach in the context of dynamical systems [15], while it addresses, from its phenomenological side, the decoupling of small scale fluctuations from their host large eddies, which break Galilean invariance. It is clear, however, that effective Lagrangian models are usually formulated at the expenses of closure assumptions (which are arbitrary, to some extent) for the dynamics of the velocity gradient tensor.

The simplest of all of the closed Lagrangian models is given by the Restricted Euler Equation, a model where viscous dissipation is neglected and the role of the pressure Hessian is taken by a velocity gradient-dependent term proportional to the identity tensor [16–19]. This model yields suggestive results on the classification of turbulent regions, based on the velocity gradient invariants Q and R [2], but is, unfortunately, affected by finite-time singularities. Ranging from linear damping to stochastic and geometric models [20–23], much has been done to solve the instability problem, which is, in fact, the main challenging issue

to be faced by competing lagrangian models. A consistent proposal, our focus in this work, is put forward by the Recent Fluid Deformation (RFD) model of Lagrangian turbulence, where dominant contributions to the pressure Hessian and the viscous term are modeled from the strained local evolution, within dissipative time scales, of advected smooth velocity gradient fields [5].

As it has been recently discussed [24], the RFD model can be recast in the Martin-Siggia-Rose (MSR) path-integral setting [25–27], so that it can be studied with the whole machinery of statistical field theoretical tools. It has been suggested, in this way, that noise renormalization, self-induced by nonlinear interactions, is the main physical mechanism one needs to consider in order to understand the onset of fat-tailed vgPDFs, as the Reynold’s number increases [24], a point further supported by numerical refinements of the original approach [28].

It is remarkable that despite the use of bold simplifying hypotheses in Ref. [24], which rely essentially on plausibility arguments, the comparison between analytical and empirical vgPDFs turns out to be very convincing. One of the simplifications consists in the use of instantons obtained from a linear truncation of the Euler-Lagrange equations; another one is the selection of a particular form for the contribution of fluctuations around the approximate saddle-point MSR action, which just renormalizes the stochastic force-force correlation term. It is interesting to call attention, in this connection, to the fact that even in the contexts of Eulerian Navier-Stokes (in two or three-dimensions) and Burgers turbulence, fluctuations around the instantons cannot be neglected at all in the derivation of the PDF tails associated to large vorticities or negative-velocity differences [29–31].

Having in mind that general lessons can be learned from the study of specific Lagrangian models of intermittency, it is of great importance to revisit the analytical treatment of the RFD model [24], in order to consolidate it as a theoretical benchmark. This is precisely our aim in this work, which clarifies what has been missed in the previous discussions and also brings to light further improvements in the description of vgPDFs.

This paper is organized as follows. In Sec. II, we briefly portray the essential phenomenological points and the defining equations of the RFD model. In Sec. III, we introduce the general MSR path-integral setting for a large class of tensorial stochastic differential equations, and apply it, in Sec. IV, to our particular problem of interest. The cumulant expansion is then found to lead to the sum of around one hundred perturbative contributions, which

are classified in order of importance, on the grounds of a power counting analysis. Next, in Sec. V, we carry out a comparison, with the help of Monte-Carlo simulations, between the empirical vgPDFs obtained from the numerical solution of the RFD stochastic differential equations and the analytical ones derived from the field theoretical approach. We also obtain the joint PDFs of the velocity gradient invariants Q and R and the local stretching exponents of marginal vgPDFs. Finally, in Sec. VI, we summarize our results and point out directions of further research.

II. THE RFD MODEL

The RFD model [5] consists of a stochastic differential approach to the onset of lagrangian intermittency as observed in the turbulent fluctuations of the lagrangian velocity gradient tensor $A_{ij}(t) \equiv \partial_j v_i$. It is straightforward to derive, as a starting point, the following integro-differential equation

$$\dot{\mathbb{A}} = V[\mathbb{A}] + g\mathbb{F} , \quad (2.1)$$

from the usual stochastic formulation of the Navier-Stokes equations, where $\dot{\mathbb{A}} \equiv d\mathbb{A}/dt$ (d/dt is the material time derivative) and $V[\mathbb{A}]$ is a nonlinear and nonlocal functional of \mathbb{A} , defined as

$$V_{ij}[\mathbb{A}] = -(\mathbb{A}^2)_{ij} + \partial_i \partial_j \nabla^{-2} \text{Tr}(\mathbb{A}^2) + \nu \nabla^2 (\mathbb{A})_{ij} . \quad (2.2)$$

In Eq. (2.1), $\mathbb{F} = \mathbb{F}(t)$ is a traceless matrix, whose entries are given by a zero-mean Gaussian stochastic processes with two-point correlators

$$\langle F_{ij}(t) F_{kl}(t') \rangle \equiv G_{ijkl} \delta(t - t') , \quad (2.3)$$

where

$$G_{ijkl} = 2\delta_{ik}\delta_{jl} - \frac{1}{2}\delta_{il}\delta_{jk} - \frac{1}{2}\delta_{ij}\delta_{kl} \quad (2.4)$$

is the most general fourth-order isotropic tensor (up to an overall prefactor) consistent with Eq. (2.1) [32]. The stochastic force strength g is proportional to the energy dissipation rate per unit mass, and will play the role of a perturbative coupling constant in our discussions.

The second and third terms in the right hand side of (2.2), denoted as the pressure Hessian and the viscous term, respectively, are the focus of modeling in Lagrangian models, where they are replaced by local algebraic functions of the velocity gradient tensor, which,

ideally, are designed to preserve important statistical properties derived from their original formulations. The closure expressions for these two contributions are, in the particular case of the RFD model, obtained from phenomenological arguments related to the short time-scale evolution of small-scale fluid blobs along lagrangian trajectories [5]. It turns out, in that way, that besides g , two time scale parameters, τ and T , respectively associated to the dissipative and integral temporal domains, completely define the model, which is assumed to describe lagrangian turbulence with Reynolds number $Re \propto (T/\tau)^2$.

The RFD model is, in concrete terms, given by the following approximation to $V[\mathbb{A}]$,

$$V(\mathbb{A}) = -\mathbb{A}^2 + \frac{\mathbb{C}^{-1}\text{Tr}\mathbb{A}^2}{\text{Tr}(\mathbb{C}^{-1})} - \frac{\text{Tr}(\mathbb{C}^{-1})}{3T}\mathbb{A}, \quad (2.5)$$

where \mathbb{C} is the Cauchy-Green tensor,

$$\mathbb{C} = \exp[\tau\mathbb{A}] \exp[\tau\mathbb{A}^T], \quad (2.6)$$

which rules the deformation of advected fluid blobs, within dissipative time scales. We have, thus, from Eq. (2.1),

$$\dot{\mathbb{A}} = V(\mathbb{A}) + g\mathbb{F} = -\mathbb{A}^2 + \frac{\mathbb{C}^{-1}\text{Tr}\mathbb{A}^2}{\text{Tr}(\mathbb{C}^{-1})} - \frac{\text{Tr}(\mathbb{C}^{-1})}{3T}\mathbb{A} + g\mathbb{F}. \quad (2.7)$$

Without loss of generality, we take $T = 1$ in the above equation. We expand, furthermore, $V(\mathbb{A})$ up to $O(\tau^2)$, which actually yields a good stage for numerical simulations of the RFD model [33]. To this order, we get

$$V(\mathbb{A}) = \sum_{p=1}^4 V_p(\mathbb{A}), \quad (2.8)$$

where

$$V_1(\mathbb{A}) = -\mathbb{A}, \quad (2.9a)$$

$$V_2(\mathbb{A}) = -\mathbb{A}^2 + \frac{\mathbb{1}}{3}\text{Tr}(\mathbb{A}^2), \quad (2.9b)$$

$$V_3(\mathbb{A}) = -\frac{\tau}{3} \left(\mathbb{A} + \mathbb{A}^T - \frac{2\mathbb{1}}{3}\text{Tr}(\mathbb{A}) \right) \text{Tr}(\mathbb{A}^2) - \frac{\tau^2}{3}\text{Tr}(\mathbb{A}^T\mathbb{A})\mathbb{A} - \frac{\tau^2}{3}\text{Tr}(\mathbb{A}^2)\mathbb{A}, \quad (2.9c)$$

$$V_4(\mathbb{A}) = -\frac{\mathbb{1}}{9}\tau^2\text{Tr}(\mathbb{A}^T\mathbb{A})\text{Tr}(\mathbb{A}^2) - \frac{\mathbb{1}}{9}\tau^2[\text{Tr}(\mathbb{A}^2)]^2 + \frac{4\mathbb{1}}{27}\tau^2[\text{Tr}(\mathbb{A})]^2\text{Tr}(\mathbb{A}^2) \\ + \frac{\tau^2}{3}\mathbb{A}^T\mathbb{A}\text{Tr}(\mathbb{A}^2) + \frac{\tau^2}{6}(\mathbb{A}^2 + \mathbb{A}^{2T})\text{Tr}(\mathbb{A}^2). \quad (2.9d)$$

Note that $V_p(\mathbb{A})$ collects velocity gradient contributions of $O(\mathbb{A}^p)$.

III. PATH-INTEGRAL FORMULATION OF STOCHASTIC LAGRANGIAN MODELS

Before we concentrate our attention on the particularities of the RFD model, as defined from Eqs. (2.7 - 2.9), it is interesting to highlight the general path-integral framework for the computation of vgPDFs in the setting of closed stochastic Lagrangian models.

Given an arbitrary stochastic differential equation for the velocity gradient tensor \mathbb{A} [34], the MSR functional formalism [25–27] can be evoked to express the conditional probability density function of finding $\mathbb{A} = \mathbb{A}_1$ at time $t = 0$, provided that $\mathbb{A} = \mathbb{A}_0$ at the initial time $t = -\beta$, as

$$\rho(\mathbb{A}_1|\mathbb{A}_0, \beta) \equiv \mathcal{N} \int_{\Sigma} D[\hat{\mathbb{A}}] D[\mathbb{A}] \exp \left\{ -S[\hat{\mathbb{A}}, \mathbb{A}] \right\}, \quad (3.1)$$

where

(i) \mathcal{N} is an unimportant normalization factor (suppressed hereafter in order to simplify notation),

(ii) the tensor field $\hat{\mathbb{A}} = \hat{\mathbb{A}}(t)$ is a time dependent auxiliary tensor field related to the tensorial noise (external stochastic forcing) \mathbb{F} ,

(iii) $\Sigma = \{\mathbb{A}(-\beta) = \mathbb{A}_0, \mathbb{A}(0) = \mathbb{A}_1\}$ is the set of boundary conditions in the above path-integral,

(iv) $S[\hat{\mathbb{A}}, \mathbb{A}]$ is the so-called MSR action,

$$S[\hat{\mathbb{A}}, \mathbb{A}] \equiv \int_{-\beta}^0 dt \left\{ i \text{Tr}[\hat{\mathbb{A}}^T L(\mathbb{A})] + \frac{g^2}{2} G_{ijkl} \hat{A}_{ij} \hat{A}_{kl} \right\}, \quad (3.2)$$

which is a complex-valued quantity, with a mathematical role analogous to the one of usual quantum mechanical actions in the Feynman path-integration formalism [35], and

(v) $L(\mathbb{A}) \equiv \dot{\mathbb{A}} - V(\mathbb{A})$. Note that in the particular case where \mathbb{A} is a solution of (2.7), then $L(\mathbb{A})$ can be identified to the external random forcing $g\mathbb{F}$.

We are interested to study vgPDFs for large asymptotic times $\beta \rightarrow \infty$, when it is natural to conjecture that a statistically stationary state for the fluctuations of the velocity gradient tensor has been reached. Assuming, furthermore, that for asymptotic times the dependence upon the initial condition \mathbb{A}_0 has vanished from the conditional vgPDFs, it proves convenient

to impose the following periodic boundary condition,

$$\mathbb{A}(0) = \mathbb{A}(-\beta) \equiv \bar{\mathbb{A}}, \quad (3.3)$$

which, as addressed in [24], leads to technical simplifications in the saddle-point approach to the MSR path-integration. The joint vgPDF for the statistically stationary state is, therefore,

$$\rho(\bar{\mathbb{A}}) = \lim_{\beta \rightarrow \infty} \rho(\bar{\mathbb{A}} | \bar{\mathbb{A}}, \beta). \quad (3.4)$$

The central idea of our analysis is that the vgPDFs are related to specific dominant flow configurations, which encode the non-linear/non-local coupling between degrees of freedom defined at different length scales, as it is clear from the structure of the Navier-Stokes equations. These prevailing configurations can be naturally addressed in the MSR path-integration formalism as the functional saddle-points of the MSR action – dubbed as the “instanton” fields $\hat{\mathbb{A}}^{sp}$ and \mathbb{A}^{sp} –, which are derived within the standard steepest descent approach [36–38] as solutions of the Euler-Lagrange equations,

$$\left. \frac{\delta S[\hat{\mathbb{A}}, \mathbb{A}]}{\delta A_{ij}} \right|_{\substack{\hat{\mathbb{A}} = \hat{\mathbb{A}}^{sp} \\ \mathbb{A} = \mathbb{A}^{sp}}} = 0 \quad \text{and} \quad \left. \frac{\delta S[\hat{\mathbb{A}}, \mathbb{A}]}{\delta \hat{A}_{ij}} \right|_{\substack{\hat{\mathbb{A}} = \hat{\mathbb{A}}^{sp} \\ \mathbb{A} = \mathbb{A}^{sp}}} = 0, \quad (3.5)$$

with the periodic boundary condition $\mathbb{A}^{sp}(0) = \mathbb{A}^{sp}(-\beta) = \bar{\mathbb{A}}$.

While the instanton fields, solutions of (3.5), can be used to devise a first approximation to the vgPDFs, fluctuations around them may be in fact relevant in order to achieve reasonable agreement with numerical or experimental results. Denoting the fluctuating fields by $\hat{\mathbb{A}}$ and \mathbb{A} , we perform the substitutions $\hat{\mathbb{A}} \rightarrow \hat{\mathbb{A}}^{sp} + \hat{\mathbb{A}}$ and $\mathbb{A} \rightarrow \mathbb{A}^{sp} + \mathbb{A}$ in the MSR action, and expand it in tensor monomials of these fields. The MSR action thus takes the form

$$S[\hat{\mathbb{A}}, \mathbb{A}] \rightarrow S[\hat{\mathbb{A}}, \mathbb{A}] = S_{sp}[\hat{\mathbb{A}}^{sp}, \mathbb{A}^{sp}] + \Delta S[\hat{\mathbb{A}}, \mathbb{A}]. \quad (3.6)$$

Note that the above expression is exact and that $S_{sp}[\hat{\mathbb{A}}^{sp}, \mathbb{A}^{sp}]$ and $\Delta S[\hat{\mathbb{A}}, \mathbb{A}]$ are the contributions to the MSR action that contain, respectively, *only* the instanton fields, and all the additional terms that involve the fluctuations \mathbb{A} and $\hat{\mathbb{A}}$. From (3.1), (3.4), and (3.6), the vgPDF can be correspondingly rewritten as

$$\rho(\bar{\mathbb{A}}) = \exp \left\{ -S_{sp}[\hat{\mathbb{A}}^{sp}, \mathbb{A}^{sp}] \right\} \int D[\hat{\mathbb{A}}] D[\mathbb{A}] \exp \left\{ -\Delta S[\hat{\mathbb{A}}, \mathbb{A}] \right\}. \quad (3.7)$$

As a well-established procedure in statistical field theory [39–41], the above path-integration over fluctuations can be perturbatively computed within the non-interacting model given by

$\Delta S_0[\hat{\mathbb{A}}, \mathbb{A}]$, defined as the quadratic contribution to the MSR action that is independent on the saddle-point solutions. We just mean that $\Delta S[\hat{\mathbb{A}}, \mathbb{A}]$ can be exactly split as

$$\Delta S[\hat{\mathbb{A}}, \mathbb{A}] = \Delta S_0[\hat{\mathbb{A}}, \mathbb{A}] + \Delta S_1[\hat{\mathbb{A}}, \mathbb{A}], \quad (3.8)$$

where ΔS_1 contains all the self-interacting terms of the MSR action. We obtain

$$\rho(\bar{\mathbb{A}}) = \exp \left\{ -S_{sp}[\hat{\mathbb{A}}^{sp}, \mathbb{A}^{sp}] \right\} \langle \exp[-\Delta S_1] \rangle_0, \quad (3.9)$$

where the expectation value $\langle \exp[-\Delta S_1] \rangle_0$ is computed in the model defined by the quadratic action ΔS_0 . If we write now, up to a normalization factor, the non-normalized vgPDF as

$$\rho(\bar{\mathbb{A}}) = \exp \left\{ -\Gamma[\hat{\mathbb{A}}^{sp}, \mathbb{A}^{sp}] \right\}, \quad (3.10)$$

then the cumulant expansion comes into play as a pragmatic way to approximate $\Gamma[\hat{\mathbb{A}}^{sp}, \mathbb{A}^{sp}]$ from the evaluation of statistical moments of ΔS_1 . Up to second order in ΔS_1 , we get

$$\begin{aligned} \Gamma[\hat{\mathbb{A}}^{sp}, \mathbb{A}^{sp}] &= S_{sp}[\hat{\mathbb{A}}^{sp}, \mathbb{A}^{sp}] + \langle \Delta S_1[\hat{\mathbb{A}}^{sp}, \mathbb{A}^{sp}] \rangle_0 \\ &\quad - \frac{1}{2} \left(\langle \Delta S_1^2[\hat{\mathbb{A}}^{sp}, \mathbb{A}^{sp}] \rangle_0 - \langle \Delta S_1[\hat{\mathbb{A}}^{sp}, \mathbb{A}^{sp}] \rangle_0^2 \right). \end{aligned} \quad (3.11)$$

The MSR effective action $\Gamma[\hat{\mathbb{A}}^{sp}, \mathbb{A}^{sp}]$ still satisfies, to first order in the perturbations, the equations of motion (3.5).

It is important to emphasize – a point of pragmatismal relevance – that it is in general difficult to find exact solutions of the saddle-point equations (3.5). This, however, should not be a matter of great concern, if one is able to find reasonable approximations for the instanton fields, since the substitution (3.6) and the second order cumulant expansion result (3.11) are always meaningful perturbative procedures in weak coupling regimes.

The cumulant expansion terms are represented in general as Feynman diagrams, and, depending on the particular model under study, they can be numerous, with variable relative weights. A power counting procedure would then be suitable to single out the most relevant diagrams.

IV. APPLICATION TO THE RFD MODEL

The approach discussed in the previous section can be straightforwardly applied to the set up of the RFD model. Following the notation introduced in (3.8), we have, for the RFD

model,

$$\Delta S_0[\hat{\mathbb{A}}, \mathbb{A}] = \int_{-\beta}^0 dt \left\{ i \text{Tr}[\hat{\mathbb{A}}^T(\dot{\mathbb{A}} + \mathbb{A}) + \frac{g^2}{2} G_{ijkl} \hat{A}_{ij} \hat{A}_{kl}] \right\} \quad (4.1)$$

and, using (2.8),

$$\begin{aligned} \Delta S_1[\hat{\mathbb{A}}, \mathbb{A}] = & -i \sum_{p=2}^4 \int_{-\beta}^0 dt \text{Tr}[(\hat{\mathbb{A}}^{sp})^T (V_p(\mathbb{A}) + \Delta V_p(\mathbb{A}))] \\ & + \text{Tr}[\hat{\mathbb{A}}^T V_p(\mathbb{A}^{sp})] + \text{Tr}[\hat{\mathbb{A}}^T (V_p(\mathbb{A}) + \Delta V_p(\mathbb{A}))], \end{aligned} \quad (4.2)$$

where

$$\Delta V_p(\mathbb{A}) = V_p(\mathbb{A}^{sp} + \mathbb{A}) - V_p(\mathbb{A}^{sp}) - V_p(\mathbb{A}) . \quad (4.3)$$

Note that if the $V_p(\mathbb{A})$ were linear functions of \mathbb{A} , we would have $\Delta V_p(\mathbb{A}) = 0$. Furthermore, it is not difficult to see that the tensor monomials in the expansion of $\Delta V_p(\mathbb{A})$ mix the instanton and the fluctuating fields.

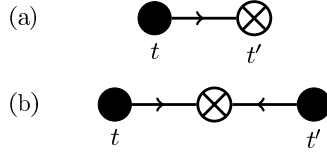


FIG. 1: The unperturbed two-point correlation functions of the RFD model, given by diagrams (a) and (b), respectively related to the time translation invariant expressions (4.5) and (4.6).

The two-point correlators (propagators) associated to the tensor fields $\hat{\mathbb{A}}$ and \mathbb{A} can be calculated through second order functional derivatives of the free-model generating functional,

$$Z[\mathbb{J}, \hat{\mathbb{J}}] = \int D[\hat{\mathbb{A}}] D[\mathbb{A}] \exp \left\{ -\Delta S_0[\hat{\mathbb{A}}, \mathbb{A}] + i \int_{-\beta}^0 dt \text{Tr}[\hat{\mathbb{J}}\mathbb{A} + \mathbb{J}\hat{\mathbb{A}}] \right\}, \quad (4.4)$$

with respect to the external source fields $\hat{\mathbb{J}}$ and \mathbb{J} , at $\hat{\mathbb{J}} = \mathbb{J} = 0$. We find, in this way, the causal propagator,

$$\langle A_{ij}(t) \hat{A}_{kl}(t') \rangle_0 = \left. \frac{\delta^2 \ln(Z[\mathbb{J}, \hat{\mathbb{J}}])}{\delta J_{ji}(t) \delta \hat{J}_{lk}(t')} \right|_{\hat{\mathbb{J}}=\mathbb{J}=0} = -i\theta(t-t') \exp(t-t) \delta_{ik} \delta_{jl} \quad (4.5)$$

and, also, the two-point velocity gradient correlation function

$$\langle A_{ij}(t) A_{kl}(t') \rangle_0 = \left. \frac{\delta^2 \ln(Z[\mathbb{J}, \hat{\mathbb{J}}])}{\delta J_{ji}(t) \delta J_{lk}(t')} \right|_{\hat{\mathbb{J}}=\mathbb{J}=0} = \frac{g^2}{4} \exp(-|t-t'|) G_{ijkl}, \quad (4.6)$$

which are represented as the Feynman diagrams illustrated in Fig. 1.

The several contributions to the MSR action that come from Eq. (4.2) yield the diagrammatic vertices that are used to build up the perturbative expansion of general correlation functions [40, 41], from the application of Wick's theorem [36, 37]. As an example, the complete set of fourth-order vertices is depicted in Fig. 2.

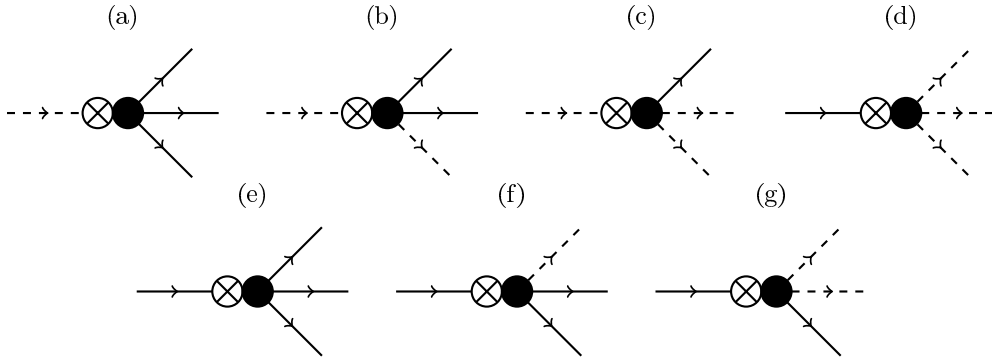


FIG. 2: Fourth-order vertices taken from the MSR action for the RFD model, Eq. (4.2). Dashed lines attached to crossed or filled circles, indicate, respectively, the insertion of the instanton fields $\hat{\mathbb{A}}^{sp}$ (dashed incoming lines) or \mathbb{A}^{sp} (dashed outgoing lines) in the perturbative vertices. Solid lines have an analogous interpretation, given in terms of the fluctuating fields $\hat{\mathbb{A}}$ and \mathbb{A} . These vertices are related to the following contributions to the MSR action (by “odd” or “even” parts of traces, we refer to the sum of tensor monomials that contain an odd or even total number of fluctuating fields): (a) $\text{Tr}[(\hat{\mathbb{A}}^{sp})^T V_3(\mathbb{A})]$, (b) odd part of $\text{Tr}[(\hat{\mathbb{A}}^{sp})^T \Delta V_3(\mathbb{A})]$, (c) even part of $\text{Tr}[(\hat{\mathbb{A}}^{sp})^T \Delta V_3(\mathbb{A})]$, (d) $\text{Tr}[\hat{\mathbb{A}}^T V_3(\mathbb{A}^{sp})]$, (e) $\text{Tr}[\hat{\mathbb{A}}^T V_3(\mathbb{A})]$, (f) odd part of $\text{Tr}[\hat{\mathbb{A}}^T \Delta V_3(\mathbb{A})]$ and (g) even part of $\text{Tr}[\hat{\mathbb{A}}^T \Delta V_3(\mathbb{A})]$.

In connection with (3.11) and (4.2), we collect one hundred and eleven Feynman diagrams that should be computed in order to get the effective MSR action up to second order in the cumulant expansion. Even though such a time consuming evaluation is likely to be within the reach of present algebraic computational methods, we can show that the vast majority of these contributions can be actually neglected in the perturbative regimes of interest. Our rationale to achieve this simplification is based on a careful determination of the powers of the coupling parameters g and τ , and also of the powers of the instanton fields associated to each one of the Feynman diagrams.

Usual graph-theoretical arguments, combined with the saddle-point equations given in (3.5), which allow us to express $\hat{\mathbb{A}}^{sp}$ in terms of \mathbb{A}^{sp} , imply that any given diagram in the

cumulant expansion with L loops, E external lines (representing $\hat{\mathbb{A}}^{sp}$ or \mathbb{A}^{sp} fields), and N_3 and N_4 vertices of types $\hat{\mathbb{A}}\mathbb{A}\mathbb{A}\mathbb{A}$ and $\hat{\mathbb{A}}\mathbb{A}\mathbb{A}\mathbb{A}\mathbb{A}$ (for $\hat{\mathbb{A}}$ and \mathbb{A} being saddle-point or fluctuating fields), respectively, is proportional to

$$g^{2(L-1)}(1 + a\tau^{N_3})\tau^{N_3+2N_4} f(\mathbb{A}^{sp}), \quad (4.7)$$

where $f(\mathbb{A}^{sp})$ is a diagram-dependent homogeneous scalar function of \mathbb{A}^{sp} with homogeneity degree E (that is $f(\alpha\mathbb{A}^{sp}) = \alpha^E f(\mathbb{A}^{sp})$, for any real positive parameter α), and a is an unimportant constant (of the order of unity). It is important to note that vertices of type $\hat{\mathbb{A}}\mathbb{A}\mathbb{A}$ do not contribute with factors that depend on their diagrammatic participation number N_2 , since these diagrams derive from V_2 contributions, which do not depend on τ , as it can be seen very clearly from Eq. (2.9b). Thus, for each Feynman diagram that takes part in the cumulant expansion, we define, taking into account (3.3) and (4.7), its ‘‘power counting coefficient’’, as

$$C(g, \tau, A) = g^{2(L-1)} \text{Max}(\tau^{N_3}, \tau^{2N_3}) \tau^{2N_4} A^E, \quad (4.8)$$

where

$$A \equiv \sqrt{\text{Tr}[\bar{\mathbb{A}}^T \bar{\mathbb{A}}]} \quad (4.9)$$

is a measure of the velocity gradient strength for the velocity gradient tensor $\bar{\mathbb{A}}$ where the vgPDF is evaluated.

With the help of Eq. (4.8), we establish, then, a rank of relevance for the diagrams of interest, as A is varied for fixed values of g and τ . In consonance with previous numerical studies [5, 24, 28, 33], we take, for the ranking analysis, $g = 1.0$ and $\tau = 0.1$. The numerical values of the power counting coefficients are inspected in the interval $0 \leq A \leq 1$, where perturbation theory is assumed to hold. The most important five contributions that appear more frequently in that range of velocity gradient strengths are labeled, in ranking order of decreasing importance, with boldface letters from **A** to **E**, and correspond to the following

cumulant expansion terms,

$$\mathbf{A}: \langle \text{Tr} \left[(\hat{\mathbb{A}}^{sp})^T V_2(\mathbb{A}) \right]_t \text{Tr} \left[(\hat{\mathbb{A}}^{sp})^T V_2(\mathbb{A}) \right]_{t'} \rangle_0 \sim A^2, \quad (4.10)$$

$$\mathbf{B}: \langle \text{Tr} \left[(\hat{\mathbb{A}}^{sp})^T V_2(\mathbb{A}) \right]_t \text{Tr} \left[\hat{\mathbb{A}}^T \Delta V_2(\mathbb{A}) \right]_{t'} \rangle_0 \sim A^2, \quad (4.11)$$

$$\mathbf{C}: \langle \text{Tr} \left[(\hat{\mathbb{A}}^{sp})^T \Delta V_2(\mathbb{A}) \right]_t \text{Tr} \left[\hat{\mathbb{A}}^T V_2(\mathbb{A}^{sp}) \right]_{t'} \rangle_0 \sim A^4/g^2, \quad (4.12)$$

$$\mathbf{D}: \langle \text{Tr} \left[(\hat{\mathbb{A}}^{sp})^T \Delta V_3(\mathbb{A}) \right]_t \text{Tr} \left[\hat{\mathbb{A}}^T V_2(\mathbb{A}^{sp}) \right]_{t'} \rangle_0 \sim A^5/g^2, \quad (4.13)$$

$$\mathbf{E}: \langle \text{Tr} \left[(\hat{\mathbb{A}}^{sp})^T V_3(\mathbb{A}) + \hat{\mathbb{A}}^T V_3(\mathbb{A}^{sp}) + \hat{\mathbb{A}}^T V_3(\mathbb{A}) \right]_t \rangle_0 = \text{const.}, \quad (4.14)$$

which have their power counting coefficients plotted in Fig. 3a. The histogram analysis of the above top five expectation values is furthermore given in Fig. 3b.

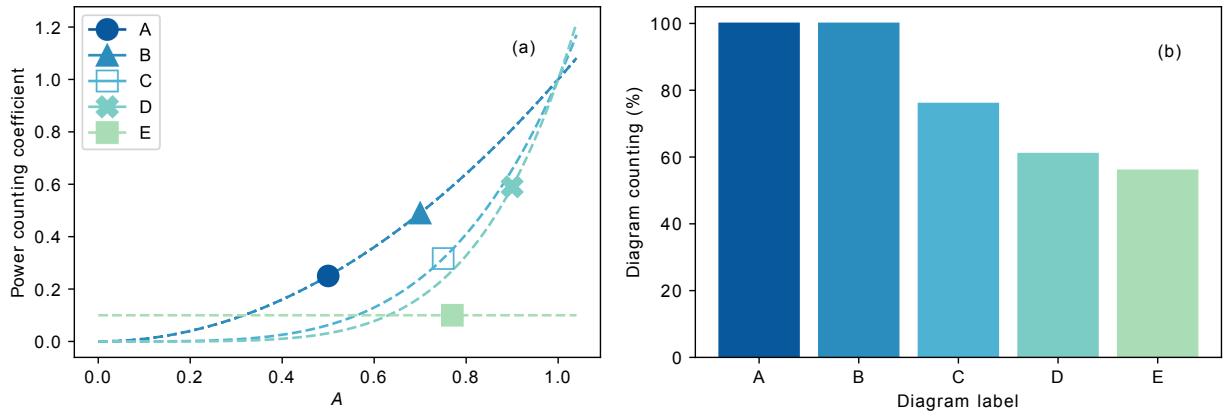


FIG. 3: (a) Plots of the power counting coefficient as a function of the velocity gradient strength A , as defined from the expectations values (4.10-4.13) taken for $g = 1.0$ and $\tau = 0.1$. (b) Relative frequencies, within the interval $0 \leq A \leq 1$, of the cases where the power counting coefficients are found to be among the first five largest ones.

It turns out that in the considered range of velocity gradient strengths, two contributions, which have exactly the same power counting coefficients, are clearly dominant over the remaining ones. These are the cumulant corrections **A** and **B**, defined in Eqs. (4.10) and (4.11). Note that the power counting coefficient for the contribution **E**, Eq. (4.14), is actually independent of A , and, therefore, plays no role at all in the evaluation of vgPDFs.

From Eq. (3.11) and the fact that $\langle \Delta S_1[\hat{\mathbb{A}}, \mathbb{A}] \rangle_0 = 0$, we conclude that the MSR effective action can be written as

$$\Gamma[\hat{\mathbb{A}}^{sp}, \mathbb{A}^{sp}] = S[\hat{\mathbb{A}}^{sp}, \mathbb{A}^{sp}] + \sum_n C_n[\hat{\mathbb{A}}^{sp}, \mathbb{A}^{sp}], \quad (4.15)$$

where n labels the several second order cumulant expansion terms $C_n[\hat{\mathbb{A}}^{sp}, \mathbb{A}^{sp}]$, which in our case are dominated by the contributions **A** and **B**. Their associated Feynman diagrams, represented in Fig. 4, are noted to renormalize the noise and propagator kernels in the effective MSR action (4.15). The contributions **A** and **B** to the effective action (4.15) can

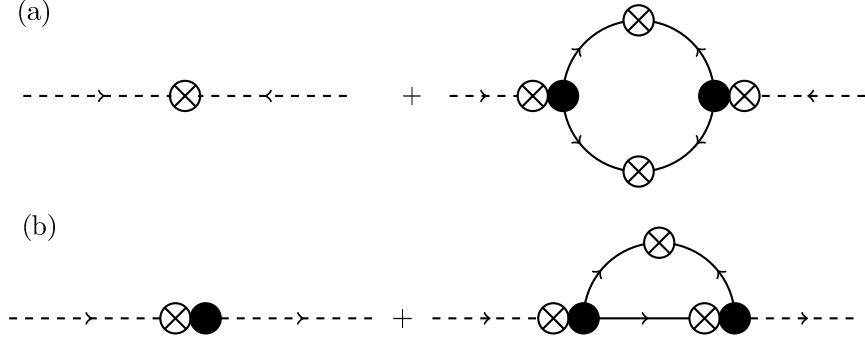


FIG. 4: Feynman diagrams for (a) the renormalized noise and (b) the renormalized causal propagator kernels, which take into account the one-loop contributions **A** and **B**, respectively.

be written, more concretely, as

$$C_{\mathbf{A}}[\hat{\mathbb{A}}^{sp}, \mathbb{A}^{sp}] = \frac{1}{2} \int_{-\beta}^0 dt \int_{-\beta}^0 dt' \hat{A}_{ij}^{sp}(t) \hat{A}_{kl}^{sp}(t') C_{ijkl}^A(t-t') \quad (4.16)$$

and

$$C_{\mathbf{B}}[\hat{\mathbb{A}}^{sp}, \mathbb{A}^{sp}] = \frac{1}{2} \int_{-\beta}^0 dt \int_{-\beta}^0 dt' \hat{A}_{ij}^{sp}(t) C_{ij}^B(\mathbb{A}^{sp}(t'), t-t'), \quad (4.17)$$

where

$$C_{ijkl}^A(t-t') = \langle [V_2(\mathbb{A}(t))]_{ij} [V_2(\mathbb{A}(t'))]_{kl} \rangle_0 \quad (4.18)$$

and

$$C_{ij}^B(\mathbb{A}^{sp}(t'), t-t') = \langle [V_2(\mathbb{A}(t))]_{ij} \hat{A}_{kl}(t') [\Delta V_2(\mathbb{A}(t'))]_{kl} \rangle_0. \quad (4.19)$$

A. Structure of the MSR Effective Action

The effective action (4.15) can be written, after the introduction of the contributions (4.16) and (4.17), as

$$\Gamma[\hat{\mathbb{A}}, \mathbb{A}] = i \int_{-\beta}^0 dt \int_{-\beta}^0 dt' \left\{ \text{Tr}[\hat{\mathbb{A}}^T(t) L^{\text{ren}}(\mathbb{A}(t'), t - t')] + \frac{g^2}{2} G_{ijkl}^{\text{ren}}(t - t') \hat{A}_{ij}(t) \hat{A}_{kl}(t') \right\}, \quad (4.20)$$

where

$$G_{ijkl}^{\text{ren}}(t - t') \equiv G_{ijkl} \delta(t - t') + C_{ijkl}^A(t - t') \quad (4.21)$$

and

$$L_{ij}^{\text{ren}}(\mathbb{A}(t'), t - t') \equiv L_{ij}(\mathbb{A}(t')) \delta(t - t') + C_{ij}^B(\mathbb{A}(t'), t - t'). \quad (4.22)$$

In contrast to the original nonperturbed MSR action (4.1), the above renormalized form (4.20) contains kernels that depend non-trivially on a pair of time instants t and t' . As it is usual (sometimes in an implicit way) in renormalization group studies [36–41], the structure of the renormalized effective action can be simplified in the case of slowly varying fields (as the instanton fields are assumed to be). This simplification is achieved through the procedure of low-frequency renormalization, which in our context consists in replacing the renormalization kernels C_{ijkl}^A and C_{ij}^B by singular ones, according to the prescriptions

$$C_{ijkl}^A(t - t') \rightarrow \tilde{C}_{ijkl}^A \delta(t - t'), \quad (4.23a)$$

$$C_{ij}^B(\mathbb{A}(t'), t - t') \rightarrow \tilde{C}_{ij}^B(\mathbb{A}(t')) \delta(t - t'), \quad (4.23b)$$

where

$$\tilde{C}_{ijkl}^A \equiv \int_{-\infty}^{\infty} dt' C_{ijkl}^A(t - t'), \quad (4.24a)$$

$$\tilde{C}_{ij}^B(\mathbb{A}(t)) \equiv \int_{-\infty}^{\infty} dt' C_{ij}^B(\mathbb{A}(t'), t - t'). \quad (4.24b)$$

Substituting (4.24a) and (4.24b) in (4.21) and (4.22), the nonperturbed and the effective MSR actions will, then, become isomorphic to each other, provided that the tensors G_{ijkl} and $L_{ij}(\mathbb{A})$ of the nonperturbed action are mapped, respectively, to the tensors

$$\tilde{G}_{ijkl}^{\text{ren}} \equiv G_{ijkl} + \tilde{C}_{ijkl}^A \quad (4.25)$$

and

$$\tilde{L}_{ij}^{\text{ren}}(\mathbb{A}) \equiv L_{ij}(\mathbb{A}) + \tilde{C}_{ij}^B(\mathbb{A}) \quad (4.26)$$

that appear in the definition of the effective renormalized action.

It is important to observe, furthermore, that from the traceless property of the stochastic forcing, it follows that $\tilde{G}_{iikl}^{\text{ren}} = \tilde{G}_{ijkk}^{\text{ren}} = 0$, and we may write, in general, that

$$\tilde{G}_{ijkl}^{\text{ren}} = D_{ijkl} - \frac{1}{3}(x + y)\delta_{ij}\delta_{kl} , \quad (4.27)$$

where

$$D_{ijkl} = x\delta_{ik}\delta_{jl} + y\delta_{il}\delta_{jk} , \quad (4.28)$$

with x and y being two independent arbitrary parameters. A straightforward computation of the noise renormalization diagram, Fig. 4a, gives us

$$\tilde{C}_{ijkl}^A = \frac{g^4}{8} \left(6\delta_{ik}\delta_{jl} - \frac{1}{4}\delta_{il}\delta_{jk} - \frac{23}{12}\delta_{ij}\delta_{kl} \right) , \quad (4.29)$$

and, as a consequence,

$$x = 2 + \frac{3}{2}g^2 , \quad y = -\frac{1}{2} - \frac{1}{16}g^2 . \quad (4.30)$$

Recalling, now, the saddle-point equations (3.5) to solve for $\hat{\mathbb{A}}^{sp}$ in terms of \mathbb{A}^{sp} , it turns out that the MSR effective action can be rewritten in a more compact way, up to the same order in perturbation expansion, as a scalar functional uniquely dependent on the velocity gradient tensor field $\mathbb{A}(t)$, namely,

$$\Gamma[\mathbb{A}] = \frac{1}{2g^2} \int_{-\beta}^0 dt [\tilde{L}_{ij}^{\text{ren}}(\mathbb{A}) D_{ijkl}^{-1} \tilde{L}_{kl}^{\text{ren}}(\mathbb{A})] , \quad (4.31a)$$

$$= \frac{a}{2g^2} \int_{-\beta}^0 dt \text{Tr}[(L^{\text{ren}}(\mathbb{A}))^T L^{\text{ren}}(\mathbb{A})] + \frac{b}{2g^2} \int_{-\beta}^0 dt \text{Tr}[L^{\text{ren}}(\mathbb{A}) L^{\text{ren}}(\mathbb{A})] , \quad (4.31b)$$

where

$$D_{ijkl}^{-1} \equiv a\delta_{ik}\delta_{jl} + b\delta_{il}\delta_{jk} , \quad (4.32)$$

with

$$a = -\frac{x}{y^2 - x^2} , \quad b = \frac{y}{y^2 - x^2} , \quad (4.33)$$

and

$$L^{\text{ren}}(\mathbb{A}) = L(\mathbb{A}) + \frac{g^2}{16}(4\mathbb{A}^T - \mathbb{A}) = \dot{\mathbb{A}} - V(\mathbb{A}) + \frac{g^2}{16}(4\mathbb{A}^T - \mathbb{A}) , \quad (4.34)$$

as it follows from the evaluation of the propagator renormalization diagram, Fig. 4b. A clear advantage of the formulation (4.31b) is that we do not need to work anymore with a coupled set of saddle-point equations like (3.5). Actually, taking into account (4.31b), it is only necessary to consider the single saddle-point equation,

$$\left. \frac{\delta\Gamma[\mathbb{A}]}{\delta A_{ij}} \right|_{\mathbb{A}=\mathbb{A}^{sp}} = 0 , \quad (4.35)$$

in order to find the instanton $\mathbb{A}^{sp}(t)$.

It is worth mentioning, in passing, that (4.31b) can be alternatively seen as an effective Onsager-Machlup action functional [42] for the RFD model.

B. Instanton Configurations

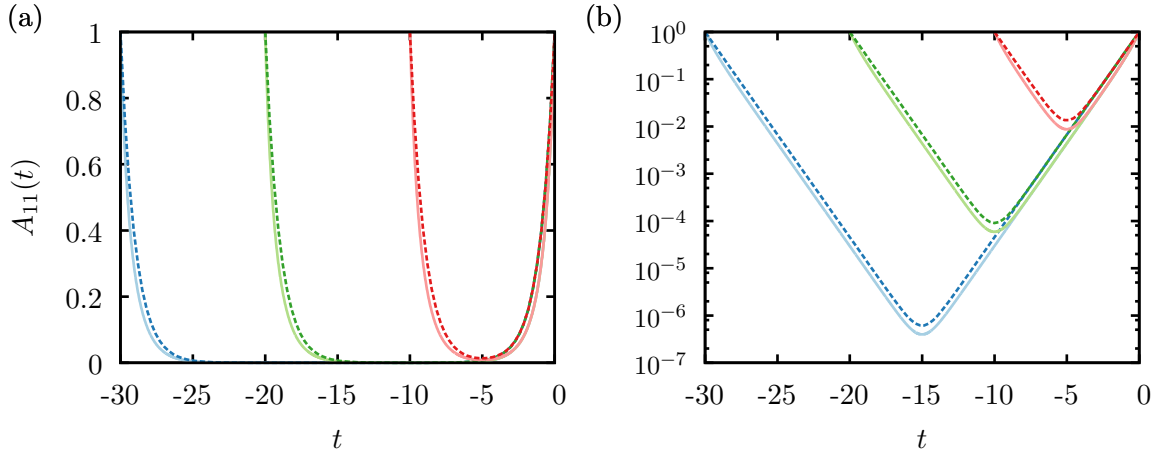


FIG. 5: Comparison between approximate (dashed lines) and numerical instantons (solid lines), obtained, respectively from Eq. (4.38) and from the application of the Chernykh-Stepanov method as discussed in Ref. [28], for $c = 1$ [that is $\bar{A}_{11} = 1$, see Eq. (4.47)], $\tau = 0.1$, and $g = 0.6$ in (a) linear and (b) monolog scales. Blue, green and red curves (left to right) correspond to $\beta = 30, 20$ and 10.

As emphasized in Sec. II, the RFD model describes the dynamics of incipient turbulent fluctuations at low Reynolds numbers. This fact suggests that the probability measure defined from $\rho(\mathbb{A})$ is not that far (in some functional sense) from a multivariate Gaussian distribution, even though heavy tails for the marginal PDFs of velocity gradient components can be clearly identified from numerical simulations of Eq. (2.7) [5]. We are motivated, thus, to devise approximate saddle-point solutions of (4.36) by working with the quadratic truncation of the renormalized effective action, that is,

$$\Gamma_0[\mathbb{A}] \equiv \frac{a}{2g^2} \int_{-\beta}^0 dt \text{Tr} \left[\dot{\mathbb{A}}^T \dot{\mathbb{A}} + \mathbb{A}^T \mathbb{A} \right] + \frac{b}{2g^2} \int_{-\beta}^0 dt \text{Tr} \left[\dot{\mathbb{A}}^2 + \mathbb{A}^2 \right]. \quad (4.36)$$

We just mean that we are interested to solve the approximate saddle-point equation

$$\left. \frac{\delta \Gamma_0[\mathbb{A}]}{\delta A_{ij}} \right|_{\mathbb{A}=\mathbb{A}^{sp}} = 0 \Rightarrow \ddot{\mathbb{A}}^{sp} - \mathbb{A}^{sp} = 0, \quad (4.37)$$

subject to the periodic boundary condition (3.3). Instanton solutions of (4.37) have the form

$$\mathbb{A}^{sp}(t) = \bar{\mathbb{A}}f(\beta, t), \quad (4.38)$$

where the time-periodic function $f(\beta, t)$, defined for $-\beta \leq t \leq 0$, is given by

$$f(\beta, t) = 2 \frac{\sinh(\beta/2)}{\sinh(\beta)} \cosh(t + \beta/2). \quad (4.39)$$

It is clear, additionally, that the vertex functions $V_p(\mathbb{A})$, being homogeneous functions of degree p , lead, according to (4.38), to

$$V(\mathbb{A}^{sp}(t)) = \sum_{p=1}^4 V_p(\bar{\mathbb{A}})[f(\beta, t)]^p. \quad (4.40)$$

Taking, now, the above expression together with (2.9) and (4.34), the effective action (4.31b) can be evaluated from the following scalar contributions,

$$\int_{-\beta}^0 dt \operatorname{Tr}[(L^{\text{ren}}(\mathbb{A}^{sp}))^T L^{\text{ren}}(\mathbb{A}^{sp})] = I_1(\beta) \operatorname{Tr}[\bar{\mathbb{A}}^T \bar{\mathbb{A}}] + \sum_{p=1}^4 \sum_{q=1}^4 I_{p+q}(\beta) H_{p,q}(\bar{\mathbb{A}}^T, \bar{\mathbb{A}}) \quad (4.41)$$

and

$$\int_{-\beta}^0 dt \operatorname{Tr}[L^{\text{ren}}(\mathbb{A}^{sp}) L^{\text{ren}}(\mathbb{A}^{sp})] = I_1(\beta) \operatorname{Tr}[\bar{\mathbb{A}}^2] + \sum_{p=1}^4 \sum_{q=1}^4 I_{p+q}(\beta) H_{p,q}(\bar{\mathbb{A}}, \bar{\mathbb{A}}), \quad (4.42)$$

where $H_{p,q}(X, Y)$ is a (computable) homogeneous scalar function of degrees p and q , related, respectively, to the matrix variables X and Y , and

$$I_1(\beta) \equiv \int_{-\beta}^0 dt [f(\beta, t)]^2, \quad I_{p+q}(\beta) \equiv \int_{-\beta}^0 dt [f(\beta, t)]^{p+q}. \quad (4.43)$$

At asymptotic times, $\beta \rightarrow \infty$, we define $I_p = \lim_{\beta \rightarrow \infty} I_p(\beta)$ to find

$$\begin{aligned} I_1 = I_2 = 1, \quad I_3 = 2/3, \quad I_4 = 1/2, \\ I_5 = 2/5, \quad I_6 = 1/3, \quad I_7 = 2/7, \quad I_8 = 1/4. \end{aligned} \quad (4.44)$$

Assembling all the above pieces together, we write the effective action as

$$\begin{aligned} \Gamma[\mathbb{A}^{sp}] &\equiv \Gamma(\bar{\mathbb{A}}) = \\ &= \frac{aI_1}{2g^2} \operatorname{Tr}[\bar{\mathbb{A}}^T \bar{\mathbb{A}}] + \frac{bI_1}{2g^2} \operatorname{Tr}[\bar{\mathbb{A}}^2] + \sum_{p=1}^4 \sum_{q=1}^4 \frac{I_{p+q}}{2g^2} [aH_{p,q}(\bar{\mathbb{A}}^T, \bar{\mathbb{A}}) + bH_{p,q}(\bar{\mathbb{A}}, \bar{\mathbb{A}})]. \end{aligned} \quad (4.45)$$

The normalized vgPDF can now be readily derived from (3.10) and (4.45), therefore, as

$$\rho(\bar{\mathbb{A}}) = \mathcal{N} \exp[-\Gamma(\bar{\mathbb{A}})] . \quad (4.46)$$

It is interesting to compare our approximate instanton solutions (4.38) with accurate numerical solutions in specific cases. As discussed in Ref. [28], diagonal velocity gradient instantons can be obtained from the application of the Chernykh-Stepanov method [43] in connection with the MSR action (3.2) for the particular boundary conditions,

$$\bar{A}_{11} = -2\bar{A}_{22} = -2\bar{A}_{33} \equiv c , \quad (4.47)$$

$$\bar{A}_{ij} = 0 \text{ for } i \neq j , \quad (4.48)$$

where c is an arbitrary constant. The approximate and the numerical instantons for $c = 1$, $\tau = 0.1$, and $g = 0.6$ are both plotted in Fig. 5, for three different values of the β parameter. As it can be clearly noticed, the approximate instantons are uniformly close to the exact ones, with very reasonable agreement

V. NUMERICAL RESULTS

We discuss, now, how the analytical predictions based on the above effective action formalism perform in the statistical modeling of turbulent velocity gradient fluctuations.

A. Marginal vgPDFs

Since (4.46) is a multivariate PDF defined on the domain of nine velocity gradient components, there is no way to evaluate it numerically from a multidimensional histogram. Partial analytical integrations which could yield marginal PDFs of A_{ij} are not feasible as well, since $\Gamma[\bar{\mathbb{A}}]$ is not quadratic. We have to resort, in this way, to the analysis of numerical statistical ensembles generated from the vgPDFs given by (4.46). They can be produced along the lines of the Monte Carlo procedure put forward in [24], where random fluctuations of A_{ij} are parametrized by an overcomplete basis of 3×3 traceless matrices.

Our Monte Carlo samples consisted of sets of 8×10^6 velocity gradient tensors, from which we extracted ensembles of 24×10^6 and 48×10^6 diagonal and off-diagonal velocity gradient components, respectively. An illustrative case for the marginal PDFs of the diagonal and

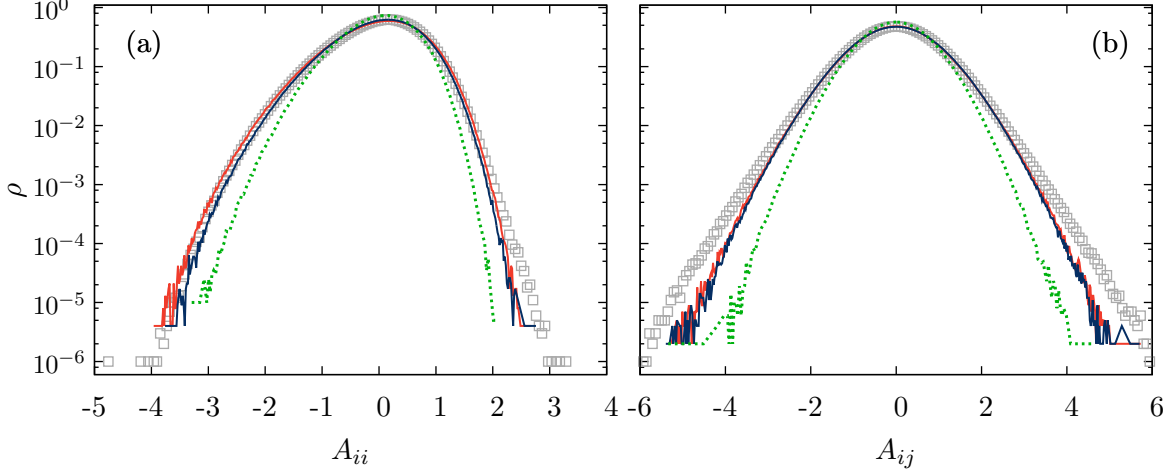


FIG. 6: PDFs for the (a) diagonal and (b) off-diagonal velocity gradient components, computed for $\tau = 0.1$ and $g = 0.8$. Open squares refer to the empirical PDFs derived from the numerical solutions of Eq. (2.7), while all the other PDFs follow from analytical expressions obtained at different improvement levels. Green dashed lines correspond to no effective action renormalization, red (light gray) lines to partial renormalization and blue (dark gray) lines to full renormalization. The diagonal and off-diagonal empirical PDFs have standard deviations and kurtosis given by $\sigma = 0.66$ and $k = 3.3$ and $\sigma = 0.89$ and $k = 3.7$, respectively.

off-diagonal components of the velocity gradient tensor is given in Fig. 6, for controlling parameters $\tau = 0.1$ and $g = 0.8$. There, we compare results for four distinct situations: PDFs obtained from

- (i) the straightforward numerical simulations of Eq. (2.7), with samples containing 10^9 velocity gradient tensors (which correspond to 2×10^5 integral times scales),
- (ii) the saddle-point MSR action with no renormalization contributions,
- (iii) the *partial renormalization* of the effective MSR action, which is renormalized by the noise contribution, and
- (iv) the *full renormalization* of the effective action, which is renormalized by both the noise and the propagator contributions.

As it can be clearly seen from Fig. 6, a great improvement is attained with the use of renormalized actions. Noise renormalization is found to be the leading contribution, and for this reason we may refer to the propagator renormalization contribution as the subleading

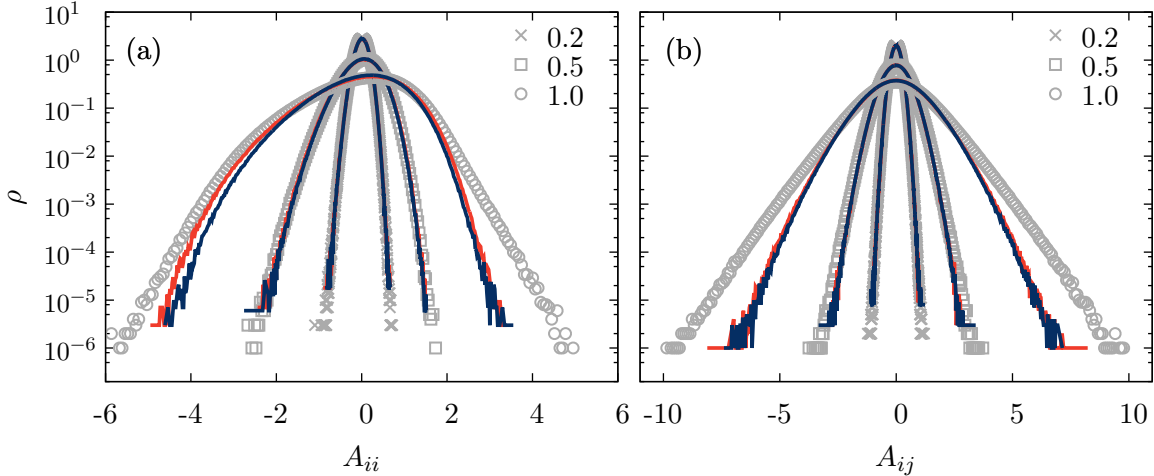


FIG. 7: PDFs for (a) the diagonal components of the velocity gradient tensor and (b) its off-diagonal components. Symbols refer to the empirical PDFs derived from the numerical solutions of Eq. (2.7), for different values of the random force strength g , as indicated in the plots; red (light gray) and blue (dark gray) lines refer, respectively, to PDFs obtained from partial and fully renormalized effective actions. For the sake of better visualization, we have not plotted the non-renormalized PDFs.

one.

When we compare the results from partial and full renormalization schemes, still focusing on Fig. 6, it seems that they would be essentially equivalent, with small differences observed, at first sight, mainly for the PDF tails of diagonal velocity gradient components. Actually, we should not be misled by visual inspection. As we will show, the core regions of these distributions, which already depart from Gaussian behavior, are much more accurately described by the PDFs obtained through fully renormalized effective actions.

A more extensive comparison between PDFs is provided in Fig. 7, where we examine cases up to the border line for the application of perturbation theory, which takes place around $g \simeq 1$, as it can be estimated from the perturbative corrections (4.30). The standard deviations and kurtoses associated to these PDFs are reported in Table I. We verify, thus, that the renormalization procedures lead in general to PDFs which closely fit the empirical ones by several standard deviations around their peaks, within the validity range of the perturbative expansion.

g	0.2		0.5		1.0		0.2		0.5		1.0	
Stat. Ens.	D	OD	D	OD	D	OD	D	OD	D	OD	D	OD
NUM	0.14	0.20	0.39	0.52	0.86	1.15	3.05	3.03	3.25	3.23	3.23	3.87
NR	0.14	0.20	0.35	0.48	0.68	0.88	3.03	3.01	3.12	3.09	3.19	3.33
PR	0.14	0.20	0.39	0.52	0.90	1.13	3.03	3.01	3.14	3.12	3.14	3.51
FR	0.14	0.20	0.39	0.52	0.84	1.13	3.03	3.01	3.14	3.10	3.14	3.39

\vdash **Standard Deviations** \vdash
Kurtoses
 \dashv

TABLE I: Standard deviations and kurtoses associated to the PDFs shown in Fig. 7. The labels D and OD stand for statistical ensembles of diagonal and off-diagonal velocity gradient components, respectively. These ensembles are characterized, besides the D/OD classification, from specifying how their associated vgPDFs are obtained, according to four alternative schemes: NUM – numerical simulations of Eq. (2.7); NR – non-renormalized saddle-point MSR actions; PR – partially renormalized effective actions; FR – fully renormalized effective actions.

B. Joint Statistics of the Velocity Gradient Invariants Q and R

The pair of velocity gradient invariants $Q \equiv -\text{Tr}(\mathbb{A}^2)/2$ and $R \equiv -\text{Tr}(\mathbb{A}^3)/3$ have been extensively used in the recent literature as important observables for the investigation of structural aspects of turbulence [2]. Turbulent flow regions can be dominated by enstrophy ($Q > 0$) or strain ($Q < 0$) and, independently, by compression ($R > 0$) or stretching ($R < 0$) dynamics. It is interesting to work with a dimensionless version of these invariants,

$$Q^* = -\frac{\text{Tr}(\mathbb{A}^2)}{2\langle \text{Tr}(S^2) \rangle} \quad \text{and} \quad R^* = -\frac{\text{Tr}(\mathbb{A}^3)}{3\langle \text{Tr}(S^2) \rangle^{3/2}}, \quad (5.1)$$

where $S = (\mathbb{A} + \mathbb{A}^T)/2$ is the usual strain rate tensor, the symmetric part of the velocity-gradient tensor. The joint PDF of Q^* and R^* shows a characteristic teardrop shape, as observed from direct numerical simulations of turbulence [16–18], and is qualitatively well reproduced by the RFD model [5]. Relying on Monte Carlo ensembles, in the same fashion as in the previous discussion on marginal vgPDFs, we find that the joint PDFs of Q^* and R^* derived from the full renormalized effective MSR action, are in excellent agreement with the ones obtained from the numerical simulation of Eq. (2.7), as it can be seen from the example given in Fig. 8.

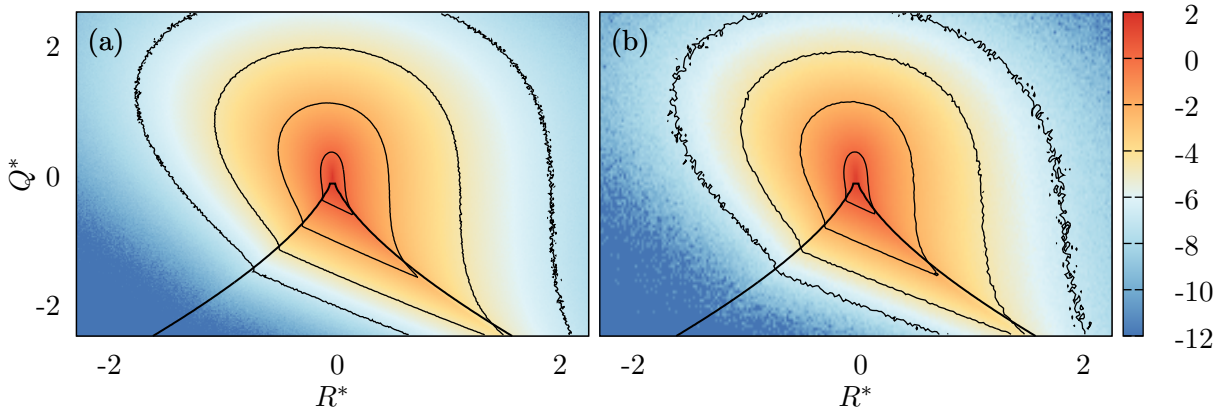


FIG. 8: Joint PDFs (and their level curves) of the velocity gradient invariants Q^* and R^* , as obtained from (a) numerical simulations of the RFD model and (b) the analytical approach based on the full renormalization of the effective MSR action. Solid lines represent the “Vieillefosse line”, defined by $(27/4)R^2 + Q^3 = 0$ (a constraint which holds for the inviscid evolution of the velocity gradient tensor). The data correspond to the RFD parameters $\tau = 0.1$ and $g = 0.5$.

C. Local Stretching Exponents

Comparisons between predicted and empirical PDFs can be sometimes a delicate issue, since both of them have to be normalized to unit, and pointwise matching can be lost, even if asymptotic expressions for their tails or cores are correctly derived from theoretical analyses. In order to test the relevance of modeling approaches, as an alternative to simple PDF fitting, one may rely on the concept of local stretching exponents, described as follows, for a non-specific PDF $\rho = \rho(\xi)$ of some real random variable ξ . Assuming that this distribution belongs to the large class of PDFs that can be written as

$$\rho(\xi) = \rho_0 \exp[-S(\xi)] , \quad (5.2)$$

where ρ_0 is just a normalization constant and $S(\xi)$ is a non-negative and monotonically increasing function of $|\xi|$, we define, then, the PDF local stretching exponent $\theta(\xi)$ as

$$\theta(\xi) = \frac{d \ln S(\xi)}{d \ln |\xi|} . \quad (5.3)$$

It is clear, from Eq. (5.3), that $S(\xi) \sim |\xi|^{\theta(\xi)}$ will hold in a local sense, if $\theta(\xi)$ is a slowly varying function of ξ .

Local stretching exponents of velocity gradient PDFs have been previously investigated in the context of Burgers turbulence at high Reynolds numbers [31]. Taking $\xi = \partial_x u$ to be the spatial velocity derivative of the Burgers one-dimensional velocity field, and $S(\xi)$ to be the saddle-point MSR action evaluated in the domain of viscous instantons [44], empirical and predicted values of $\theta(\xi)$ were then compared in Ref. [31] for the PDF tails that describe large negative fluctuations of ξ .

It is interesting to address a similar discussion in the RFD model, where ξ can be taken to be a diagonal or a off-diagonal component of the velocity gradient tensor. It is important, however, to note that the discussion of Ref. [31] focused on velocity gradient domains where the perturbative analysis of fluctuations around the instanton solutions breaks down. In this work, on the other hand, our attention is centered on the perturbative non-Gaussian deviations of the vgPDF shapes at the onset of turbulence. This means, as a counterpart, that if we attempt to define local stretching exponents for the PDFs of diagonal and off-diagonal velocity gradients from a straightforward application of Eq. (5.3), we would run in trouble, since both the saddle-point or renormalized MSR actions vanish for vanishing velocity gradients, a fact that would render the evaluation of $\theta(\xi)$ problematic for small values of ξ .

In order to bypass these difficulties, we introduce the modified local stretching exponent $\vartheta(\xi)$ as follows

$$\vartheta(\xi) = -\frac{d \ln \rho(\xi)}{d \ln |\xi|} . \quad (5.4)$$

Considering that within the PDF cores $\theta(\xi)$ is slowly varying, we get

$$\vartheta(\xi) \simeq \theta(\xi) S(\xi) = \theta(\xi) \ln \left(\frac{\rho_0}{\rho(\xi)} \right) , \quad (5.5)$$

where, above, ξ represents an arbitrary component of the velocity gradient tensor. Eq. (5.4) can be used, therefore, to produce rigorous validity tests of the instanton approach to the RFD model, since $\vartheta(\xi)$ depends, as particularly indicated by Eq. (5.5), on different defining aspects of the probability distribution $\rho(\xi)$.

Paying careful attention to the robustness of results, we have used high-order B-splines to interpolate the marginal vgPDFs, in such a way that it is not necessary to worry with numerical errors that could be associated to the derivative operation in Eq. (5.4). We recall, now, that the pointwise error in determining a general PDF $\rho(\xi)$ from uncorrelated

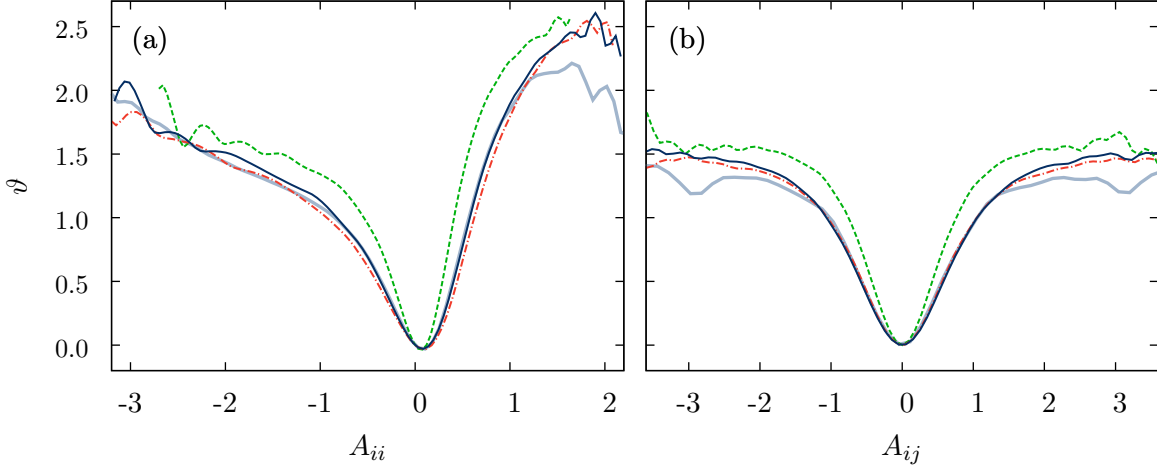


FIG. 9: Modified local stretching exponents for the PDFs of (a) diagonal and (b) off-diagonal velocity gradient components, evaluated for the RFD model with controlling parameters $\tau = 0.1$ and $g = 0.8$. Stretching exponents are evaluated for PDFs derived from (i) the numerical solution of the RFD stochastic equations (gray lines), (ii) the saddle-point MSR action (dashed green lines), (iii) partially renormalized effective MSR actions (dashed-dotted red lines), and (iv) fully renormalized effective MSR actions (dark blue lines).

numerical data is

$$\sigma_\rho(\xi) = \sqrt{\frac{\rho(\xi)(1 - \rho(\xi)\delta)}{N\delta}} \simeq \sqrt{\frac{\rho(\xi)}{N\delta}}, \quad (5.6)$$

where δ is the bin size and N is the number of elements in the numerical samples. The meaning of (5.6), when working with smooth interpolations, like the ones given by B-splines, is that the estimated PDF can be written, in principle, as

$$\rho(\xi) = \bar{\rho}(\xi) + \phi(\xi)\sigma_{\bar{\rho}(\xi)}, \quad (5.7)$$

where $\bar{\rho}(\xi)$ denotes the exact (unknown) PDF, and the modulating function $\phi(\xi)$, with $|\phi(\xi)| < 1$, is assumed to be as smooth as $\sigma_{\bar{\rho}(\xi)}$, that is $|\phi'/\phi| \simeq |\sigma'_{\bar{\rho}(\xi)}/\sigma_{\bar{\rho}(\xi)}| = |\bar{\rho}'/\bar{\rho}|/2$.

From Eqs. (5.4), (5.6), and (5.7), we find, thus, that the propagated uncertainty in the evaluation of $\vartheta(\xi)$ has the upper bound

$$\sigma_\vartheta(\xi) = \vartheta(\xi) \frac{3\sigma_\rho(\xi)}{4\rho(\xi)} = \vartheta(\xi) \frac{3}{4\sqrt{N\delta\rho(\xi)}}. \quad (5.8)$$

Taking $N \geq 24 \times 10^6$, $\delta \simeq 0.1$, and $\rho(\xi) > 0.1$ within the PDFs cores (see Fig. 7), it follows that

$$\frac{\sigma_\vartheta(\xi)}{\vartheta(\xi)} < 1.5 \times 10^{-3}, \quad (5.9)$$

so that the modified local stretching exponents are in fact determined with excellent precision in the velocity gradient domains of interest.

As it can be seen from Fig. 9, while both partially or fully renormalized effective MSR actions lead to equivalent accurate predictions for the stretching exponents $\vartheta(\xi)$ of the PDFs of off-diagonal velocity gradient components, the diagonal case is only accurately modeled by the full renormalization scheme in the range $|A_{ii}| < 1$. Partial renormalization yields, for the diagonal case, predictions missing the empirical values of $\vartheta(\xi)$ in the PDF core region by systematic errors of the order of 5%, which, according to (5.9), are considerably greater than the standard deviations of measurement precision.

As the velocity gradients increase in absolute value, we note, from Fig. 9, that the accurate agreement between the predicted and the empirical stretching exponents ends in a somehow abrupt way, even before their evaluations become unreliable. The main reason underlying this phenomenon is the unavoidable breakdown of the perturbative expansion around instantons, when cumulants of higher orders cannot be neglected anymore in comparison with the second order contributions (4.16) and (4.17).

VI. CONCLUSIONS

This work provides a detailed report on the field theoretical approach to the problem of lagrangian intermittency, as described along the lines of the RFD model [5]. Motivated by the promising results advanced in Ref. [24], we found that the analytical expressions for the vgPDFs can be further improved from the consideration of additional contributions to the renormalized MSR effective action, which rely, ultimately, on the cumulant integration of fluctuations around instanton configurations.

It is important to emphasize that the present formalism - not restricted at all to the specific case of the RFD model - yields accurate results for the core regions (defined within a few standard deviations around central peaks) of vgPDFS, at the onset of turbulence, when fat tails start to show up. This is due to the fact that under such conditions the perturbative treatment is feasible, so that the usual cumulant expansion method can be applied with confidence. At the far PDF tails, on the other hand, the perturbative expansion breaks down, but, as a counterpart, the role of fluctuations is assumed to be less relevant than the one at the PDF cores.

A particularly interesting aspect in having analytical expressions for vgPDFs is that they are joint PDFs, and, in this way, may be used to generate Monte Carlo ensembles for the analysis of conditioned statistics phenomena (like the alignment correlations between vorticity and the strain principal axes [2]), which can be considerably larger than the corresponding ensembles produced from the straightforward numerical solution of modeling stochastic equations.

Extensions of the analytical methodology discussed in this work to other stochastic hydrodynamic systems, as the Burgers model or three-dimensional turbulence, as well as the recent improved variations of the RFD model [45, 46], offer no major conceptual difficulties and are deserved for future research.

Acknowledgments

G.B.A. and L.M. thank CNPq for financial support. R.M.P. thanks CAPES and FACEPE for financial support and L. S. Grigorio for interesting discussions. G.B.A. also thanks M. Moriconi for useful discussions.

-
- [1] G.K. Batchelor and A.A. Townsend, Proc.R. Soc. London A **99**, 238 (1949).
 - [2] A. Tsinober, *An Informal Conceptual Introduction to Turbulence*, Springer Netherlands (2009).
 - [3] U. Frisch, *Turbulence: The Legacy of A. N. Kolmogorov*, Cambridge University Press (1995).
 - [4] L. Chevillard, B. Castaing, E. L ev eque, and A. Arneodo, Physica D **218**, 77 (2006).
 - [5] L. Chevillard and C. Meneveau, Phys. Rev. Lett. **97**, 174501 (2006).
 - [6] P. Vukoslavcevic, J.M. Wallace, and J.L. Balint, J. Fluid Mech. **228**, 25 (1991).
 - [7] J.M. Wallace, Phys. Fluids **21**, 021301 (2009).
 - [8] J.M. Wallace and P.V. Vukoslavcevic, Ann. Rev. Fluid Mech. **42**, 157 (2010).
 - [9] J. Katz and J. Sheng, Ann. Rev. Fluid Mech. **42**, 531 (2010).
 - [10] A. Tsinober, E. Kit, and T. Dracos, J. Fluid Mech. **242**, 169 (1992).
 - [11] B.W. Zeff, D.D. Lanterman, R. McAllister, R. Roy, E.J. Kostelich, and D. P. Lathrop, Nature **421**, 146 (2003).

- [12] M. Kholmyansky, L. Moriconi, R. M. Pereira, and A. Tsinober, *Phys. Rev. E* **80**, 036311 (2009).
- [13] Z.-S. She and E. Leveque, *Phys. Rev. Lett.* **72**, 336 (1994).
- [14] B. Dubrulle, *Phys. Rev. Lett.* **73**, 959 (1994).
- [15] P. Holmes, J.L. Lumley, and G. Berkooz, *Turbulence, Coherent Structures, Dynamical Systems and Symmetry*, Cambridge University Press (1998).
- [16] J. Léorat, *La Turbulence Magnétohydrodynamique Hélicitaire et Génération des Champs Magnétique a Grande Échelle*, PhD Thesis, Univ. Paris VII (1975).
- [17] P. Vieillefosse, *J. Phys.* **43**, 837 (1982).
- [18] P. Vieillefosse, *J. Phys. A* **25**, 837 (1984).
- [19] C. Meneveau, *Ann. Rev. Fluid Mech.* **43**, 219 (2011).
- [20] J. Martin, C. Dopazo, and L. Valino, *Phys. Fluids* **10**, 2012 (1998).
- [21] S.S. Girimaji and S.B. Pope, *Phys. Fluids A* **2**, 242 (1990).
- [22] M. Chertkov, A. Pumir, and B. I. Shraiman, *Phys. Fluids* **11**, 2394 (1999).
- [23] E. Jeong and S. S. Girimaji, *Comp. Fluid Dyn.* **16**, 421 (2003).
- [24] L. Moriconi, R.M. Pereira, and L.S. Grigorio, *J. Stat. Mech.* **10**, P10015 (2014).
- [25] P.C. Martin and E.D. Siggia and H.A. Rose, *Phys. Rev. A* **8**, 423 (1973).
- [26] C. de Dominicis, *J. Phys. Colloques C1* **37**, 247 (1976).
- [27] H.K. Janssen, *Z. Phys. B* **23**, 377 (1976).
- [28] L.S. Grigorio, F. Bouchet, R.M. Pereira, and L. Chevillard, *J. Phys A* **50**, 055501 (2017).
- [29] L. Moriconi, *Phys. Rev. E* **70**, 025302(R) (2004).
- [30] G. Falkovich and V. Lebedev, *Phys. Rev. E* **83**, 045301(R) (2011).
- [31] T. Grafke, R. Grauer, T. Schäfer, and E. Vanden-Eijnden, *Europhys. Lett.* **109**, 34003 (2015).
- [32] S.B. Pope, *Turbulent Flows*, Cambridge University Press (2000).
- [33] M.M. Afonso and C. Meneveau, *Physica D* **239**, 1241 (2010).
- [34] We have in mind the large class of additive noise models, but our arguments can be straightforwardly extended to the cases of stochastic differential equations with multiplicative noise.
- [35] R.P. Feynman and A.R. Hibbs, *Quantum Mechanics and Path Integrals*, Dover Publications Inc. (2005).
- [36] D.J. Amit, *Field Theory, the Renormalization Group, and Critical Phenomena*, World Scientific (1984).

- [37] J. Zinn-Justin, *Quantum Field Theory and Critical Phenomena*, Clarendon Press (2002).
- [38] M.E. Peskin and D.V. Schroeder, *An Introduction to Quantum Field Theory*, Addison-Wesley Publishing Company (1995).
- [39] J.B. Kogut, *Rev. Mod. Phys.* **51**, 659 (1979).
- [40] A.L. Barabási and H.E. Stanley, *Fractal Concepts in Surface Growth*, Cambridge University Press (1995).
- [41] M. Kardar, *Statistical Physics of Fields*, Cambridge University Press (2007).
- [42] L. Onsager and S. Machlup, *Phys. Rev.* **91**, 1505 (1953).
- [43] A.I. Chernykh and M.G. Stepanov, *Phys. Rev. E* **64**, 026306 (2001).
- [44] E. Balkovsky, G. Falkovich, I. Kolokolov, and V. Lebedev, *Phys. Rev. Lett.* **78**, 1452 (1997).
- [45] P. L. Johnson and C. Meneveau, *J. Fluid Mech.* **804**, 387 (2016).
- [46] R. M. Pereira, L. Moriconi, and L. Chevillard, *A multifractal model for the velocity gradients dynamics in turbulent flows*, <https://arxiv.org/abs/1705.09843> (2017).